

## Supplementary information

### **Novel highly emissive *H*-aggregates with aggregate fluorescence change in phenylbenzoxazole-based system**

**Lianke Wang, Yanfang Shen, Weinan Xu, Qiuju Zhu, Jieying Wu, Yupeng Tian, Hongping Zhou\***

*College of Chemistry and Chemical Engineering, Anhui University, Hefei 230601, P. R. China.*

*Fax: +86-551-63861259; Tel: +86-551-63861259; E-mail: [zhpzhp@263.net](mailto:zhpzhp@263.net)*

## Experimental Section

### Materials and apparatus

PPA, 4-diethylaminobenzaldehyde, salicylaldehyde, 4-(diethylamino)salicylaldehyde, *o*-aminophenol were purchased from Aladdin, the other chemicals were available commercially and used without further purification. Avarian liquid-state NMR operated at 400 MHz for <sup>1</sup>H NMR and 100 MHz for <sup>13</sup>C NMR was used for NMR spectra measurements, using DMSO-*d*<sub>6</sub> as solvent. Chemical shifts were reported in parts per million (ppm) relative to internal TMS (0 ppm) and coupling constants in Hz. Splitting Patterns were described as singlet (*s*), doublet (*d*), triplet (*t*), quartet (*q*), or multiplet (*m*). The mass spectra were obtained on Bruker Autoflex III smartbeam MALDI-TOF/TOF mass spectrometer. The one-photon absorption (OPA) spectra were recorded on the UV-265 spectrophotometer. The one-photon excited fluorescence (OPEF) spectra measurements were performed using the Hitachi F-7000 fluorescence spectrophotometer. OPA and OPEF of **2a-2c** were measured in ethanol with the concentration of 10 mM. The quartz cuvettes used were of 1cm path length. Crystallographic data (excluding structure factors) for the structure (*s*) reported in this paper have been deposited with the Cambridge Crystallographic Data Centre as supplementary publication no. CCDC: 994632-994634. Thermal transitions were studied by differential scanning calorimetry (DSC-2000) and thermogravimetric analysis (TGA-2000) at a heating rate of 20 K·min<sup>-1</sup> under nitrogen. The scanning electron microscope (SEM) images were taken on a S4800 (Hitachi, Japan) scanning electron microscope.

### Theoretical calculations

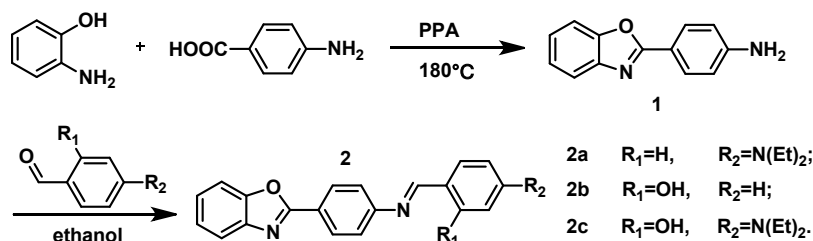
We calculated frontier molecular orbital (Figure S10) using time-dependent density functional theory (TD-DFT) method at B3LYP/6-31G basis in the Gaussian 03 E01 package. The excitation energies, oscillator strengths, corresponding wavelengths and main configurations for the most relevant singlet excited states were listed in Table S2. Their electron clouds of both the highest-occupied molecular orbital (HOMO) and lowest unoccupied molecular orbital (LUMO) are distributed evenly along the long axis of the molecule, which reveals that their optical transitions can attribute to the HOMO level to LUMO level transitions. According to the distribution of electron clouds of HOMO and LUMO level, the absorption and emission of **2b** can attribute to  $\pi$ - $\pi^*$  transitions, the absorption and emission of **2a** and **2c** are ascribed to intramolecular charge transfer (ICT) from *N,N*-diethyl groups to benzoxazolyl groups, accompanying with  $\pi$ - $\pi^*$  transitions.

### Preparation of aggregates

Stock DMF solutions of the molecules with a concentration of 10 mM were prepared. An aliquot (25  $\mu$ L) of this stock solution was transferred to a 5 mL volumetric flask. After adding an appropriate amount of ethanol, water was added under vigorous stirring to furnish 5 mL ethanol-H<sub>2</sub>O mixtures with water fractions (*f<sub>w</sub>*) of 0-90 vol%. The UV-vis spectra and emission spectra of the resultant mixtures were measured immediately.

### Synthesis

Three compounds **2a**, **2b** and **2c** were prepared according to the synthetic routes shown in **Scheme S1**. Detailed procedures and characterization can be found in the following.



**Scheme S1.** Synthetic routes to **2a**, **2b** and **2c**.

**(E)N,N-Diethyl-4-[4'-(benzoxazolyl)]benzylideneimine (2a).** *p*-(benzoxazolyl)aniline was obtained from the condensation of *o*-aminophenol with *p*-aminobenzoic acid in the presence of polyphosphoric acid.<sup>17</sup> 4-diethylaminobenzaldehyde (0.48 g, 2.7 mmol) was added dropwise into 20 mL ethanol solution of *p*-(benzoxazolyl)aniline (0.57 g, 2.7 mmol). The mixed solution was stirred at ambient temperature, and yellow solid precipitated gradually after 0.5 h. The solid was filtrated after the reaction completed and recrystallized with ethanol to produce 0.846 g light yellow solid and yield 80.57%. mp: 139.9 °C. <sup>1</sup>H NMR (400 MHz, DMSO-*d*<sub>6</sub>, δ): 9.63 (s, 1H), 7.85-7.87 (d, *J* = 7.2 Hz, 2H), 7.64-7.66 (d, *J* = 7.2 Hz, 4H), 7.34-7.30 (m, 2H), 6.75-6.77 (d, *J* = 8.0 Hz, 1H), 6.71-6.69 (d, *J* = 7.6 Hz, 1H), 3.46-3.41 (q, *J* = 6.8 Hz, 4H), 1.14-1.11 (t, *J* = 0.4 Hz, 6H). <sup>13</sup>C NMR (400 MHz, DMSO-*d*<sub>6</sub>, δ): 189.41, 163.57, 152.48, 151.91, 149.86, 142.09, 131.85, 128.91, 124.29, 123.98, 118.69, 113.52, 112.73, 110.57, 110.20, 43.93, 12.27. MALDI-TOF calcd for [M], 369.18, found, 369.50.

**(E)2-hydroxy-4-[4'-(benzoxazolyl)]benzylideneimine (2b).** The orange crystalline solid **2b** was prepared according to a similar procedure of **2a** using salicylaldehyde (0.33 g, 2.7mmol) instead of 4-diethylaminobenzaldehyde and yield 89.10%. mp: 235.8 °C. <sup>1</sup>H NMR (400 MHz, DMSO-*d*<sub>6</sub>, δ): 10.26 (s, 1H), 7.87-7.81 (q, *J* = 6.8 Hz, 3H), 7.66-7.64 (m, 4H), 7.54-7.43 (m, 3H), 7.34-7.30 (m, 2H), 6.00 (s, 1H). <sup>13</sup>C NMR (400 MHz, DMSO-*d*<sub>6</sub>, δ): 166.45, 163.48, 160.68, 152.34, 142.05, 136.34, 129.10, 128.92, 124.28, 123.91, 122.42, 122.25, 119.45, 118.70, 117.11, 113.56, 112.74, 110.18. MALDI-TOF calcd for [M+H]<sup>+</sup>, 314.11, found, 315.80.

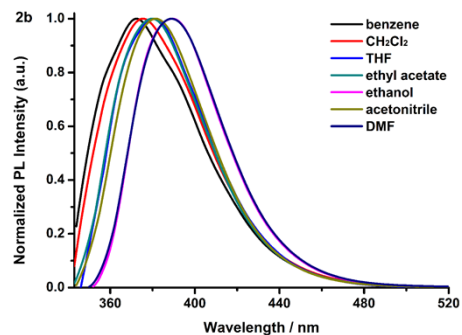
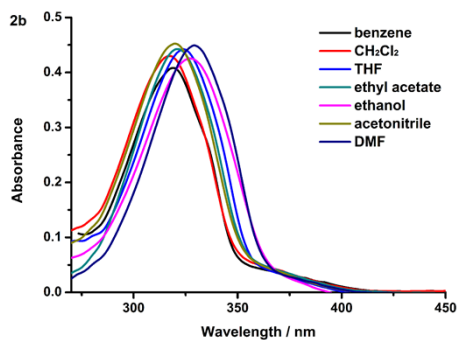
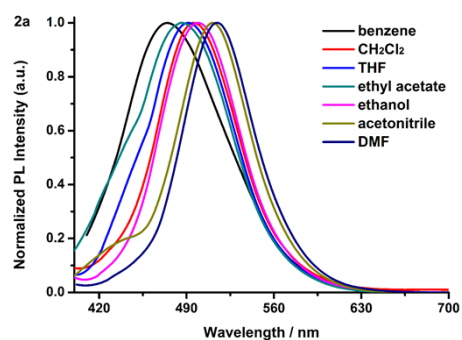
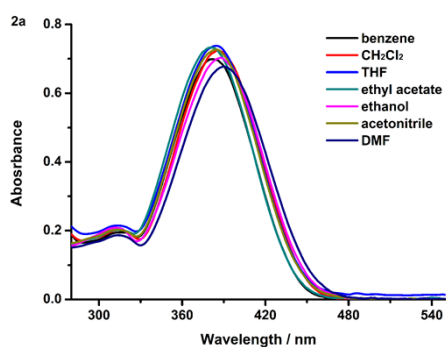
**(E)N,N-Diethyl-2-hydroxy-4-[4'-(benzoxazolyl)]benzylideneimine (2c).** The golden yellow crystalline solid **2c** was prepared according to a similar procedure of **2a** using 4-(diethylamino)salicylaldehyde (0.52 g, 2.7mmol) instead of 4-diethylaminobenzaldehyde and yield 74.47%. mp: 201.9 °C. <sup>1</sup>H NMR (400 MHz, DMSO-*d*<sub>6</sub>, δ): 9.61 (s, 1H), 8.24-8.22 (d, *J* = 7.6, 1H), 7.87-7.79 (m, 2H), 7.66 (s, 1H), 7.56-7.54 (d, *J* = 7.6 Hz, 1H), 7.45-7.28 (m, 3H), 6.70-6.68 (d, *J* = 8.4 Hz, 1H), 6.38-6.34 (t, *J* = 9.8 Hz, 1H), 6.10-6.00 (m, 2H), 3.44-3.39 (q, *J* = 6.8 Hz, 4H), 1.15-1.10 (q, *J* = 7.6 Hz, 6H). <sup>13</sup>C NMR (400 MHz, DMSO-*d*<sub>6</sub>, δ): 163.56, 163.36, 153.76, 152.50, 149.83, 142.06, 133.99, 128.92, 128.58, 124.30, 123.99, 118.69, 113.49, 112.66, 111.16, 110.22, 104.43, 95.86, 44.08, 12.38. MALDI-TOF calcd for [M+H]<sup>+</sup>, 385.46, found, 386.41.

Table S1. Spectroscopic Data of **2a-2c**.

	solvents	$\lambda_{\text{max}}^a$	$\epsilon_{\text{max}}^b$	$\lambda_{\text{max}}^c$	$\Delta\nu^d$
<b>2a</b>	benzene	381.5	6.99	475	5159.688
	CH <sub>2</sub> Cl <sub>2</sub>	385.5	7.24	495	5738.317
	THF	384	7.38	492	5716.463
	ethyl acetate	380.5	7.32	486	5705.077
	ethanol	388	7.03	499	5733.116

<b>2b</b>	acetonitrile	384	7.27	511	6472.195
	DMF	390	6.78	514	6185.773
	benzene	319	4.08	372	4466.242
	CH <sub>2</sub> Cl <sub>2</sub>	317	4.30	376	4949.997
	THF	324	4.42	381	4617.478
	ethyl acetate	321	4.43	380	4836.859
	ethanol	327	4.25	389	4874.099
<b>2c</b>	acetonitrile	320	4.52	381	5003.281
	DMF	329	4.49	389	4688.196
	benzene	401.5	6.33	489	4456.702
	CH <sub>2</sub> Cl <sub>2</sub>	405	6.26	490	4283.195
	THF	403	6.46	490	4405.733
	ethyl acetate	402.5	6.84	485	4226.164
	ethanol	414.5	6.59	495	3717.289
acetonitrile	401.5	6.81	496	4745.310	
DMF	410.5	6.37	498	4280.215	

<sup>a</sup> Absorption peak position in nm ( $1 \times 10^{-5} \text{ mol L}^{-1}$ ). <sup>b</sup> Maximum molar absorbance in  $10^4 \text{ mol}^{-1} \text{ L cm}^{-1}$ . <sup>c</sup> Peak position of emission in nm ( $1.0 \times 10^{-5} \text{ mol L}^{-1}$ ), excited at the absorption maximum. <sup>d</sup> Stokes shift in nm.



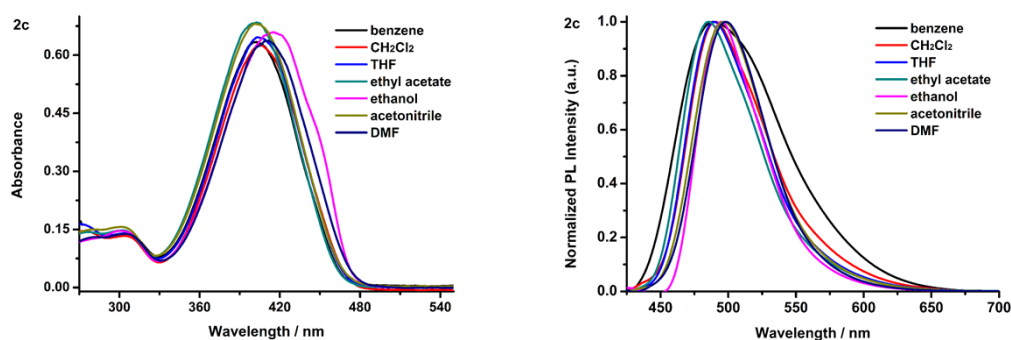


Figure S1. The absorption and normalized PL spectra of **2a-2c** in seven organic solvents of different polarities with a concentration of  $1 \times 10^{-5} \text{ mol L}^{-1}$ .

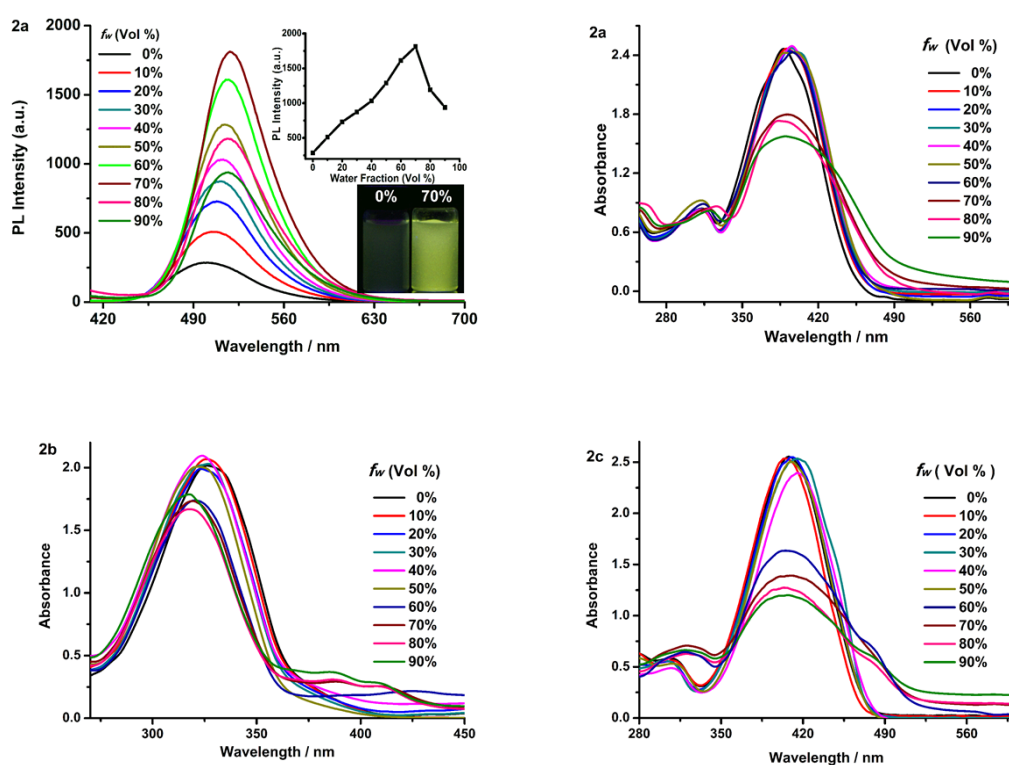


Figure S2. The absorption and PL spectra of **2a-2c** in ethanol/water mixtures with different water fraction ( $f_w$ ). Photos taken under UV light of **2b** and **2c** in different  $f_w$  ethanol/water mixtures. Concentration:  $50 \mu\text{M}$ .

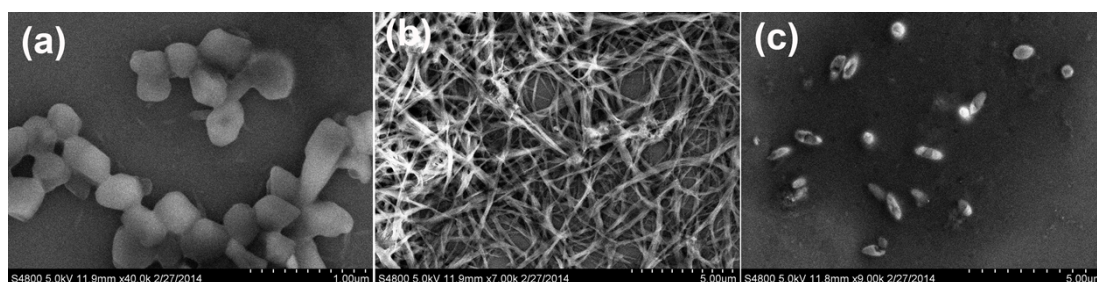


Figure S3. SEM images of (a). **2a**, (b). **2b** and (c). **2c** in ethanol/water mixtures at concentrations of  $50 \mu\text{M}$  with  $f_w=80\%$ .

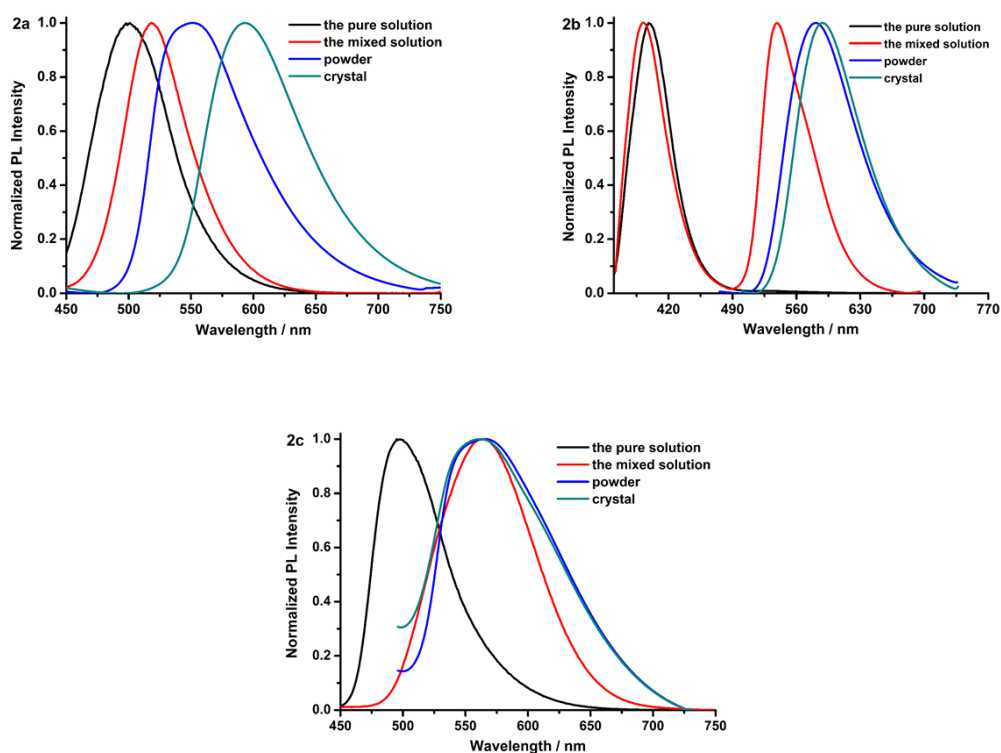


Figure S4. Normalized PL spectra of **2a-2c** in the different states: the pure solvent, the mixed solution with  $f_w = 90\%$ , the powder and the crystal.

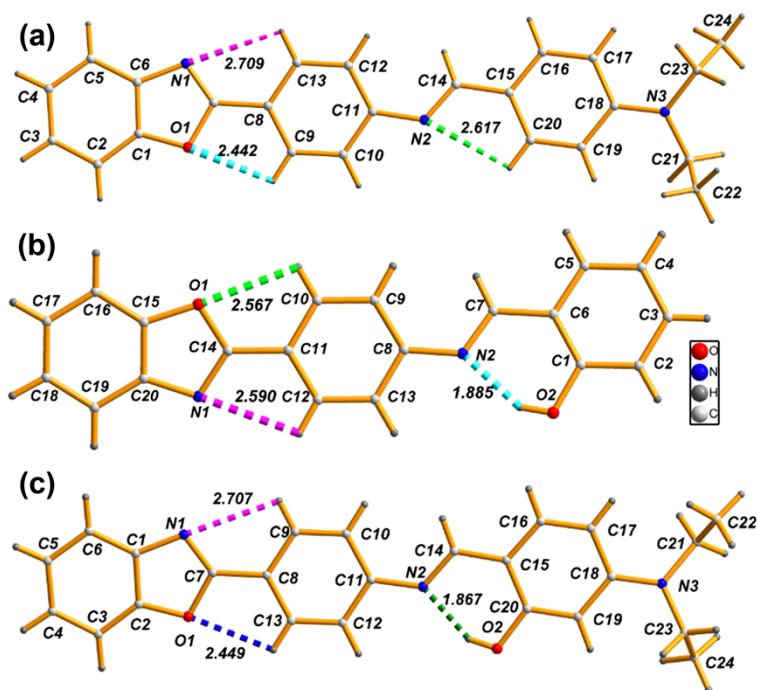


Figure S5. The single molecular structure of (a) **2a**, (b) **2b** and (c) **2c** showing the intramolecular interactions.

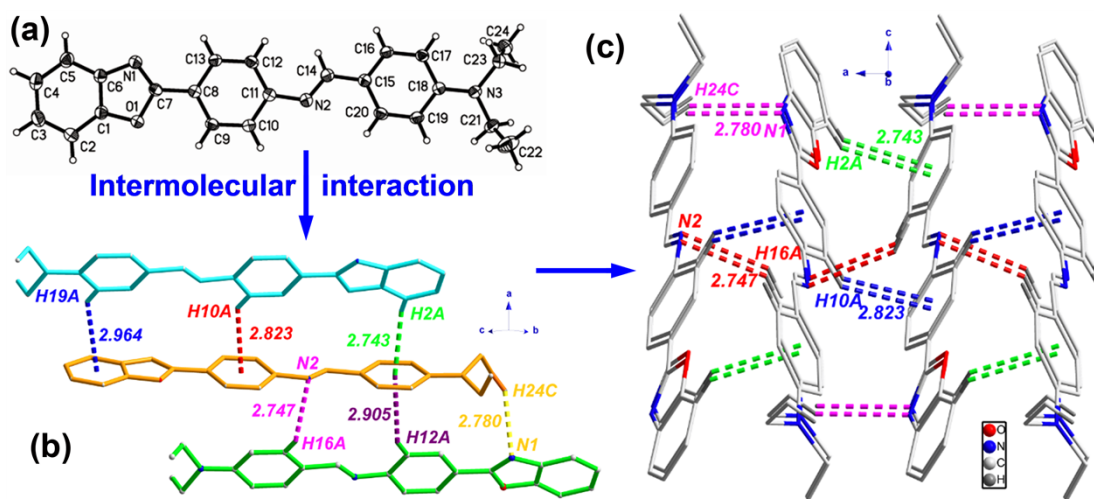


Figure S6. (a) ORTEP drawing of **2a**. (b) The one dimensional band structure of **2a** formed by multiple intermolecular C-H $\cdots$  $\pi$  and hydrogen bonds interactions. (c) Two dimensional layer structure of **2a** in the crystal structure. Dotted colorful lines represent the weak interactions. Hydrogen atoms not participating in hydrogen bonds are omitted for clarity.

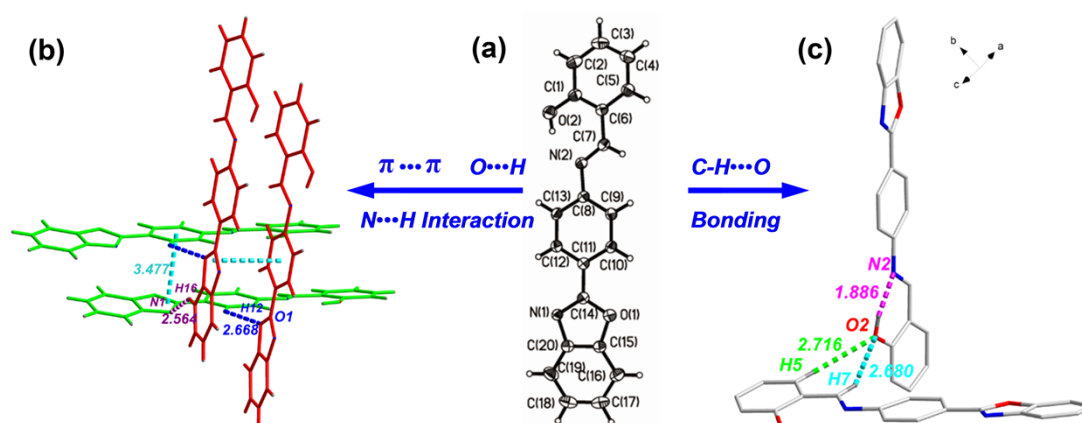


Figure S7. (a) ORTEP drawing of **2b**. (b) The cross stacking #-shaped structure of complex **2b** via intermolecular hydrogen bonds and  $\pi\cdots\pi$  interaction. (c) The cross stacking L-shaped structure of complex **2b** via C-H $\cdots$ O hydrogen bonds. Dotted colorful lines represent the weak interactions. Hydrogen atoms not participating in hydrogen bonds are omitted for clarity.

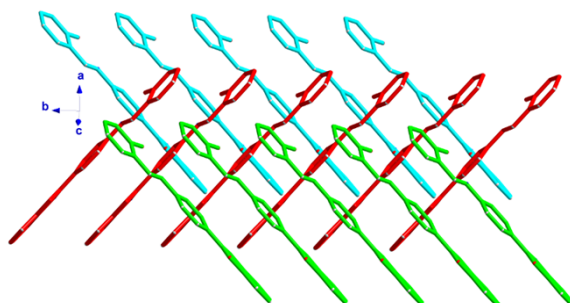


Figure S8. The two dimensional cross-stacked layer structure of **2b** in the crystal. All the hydrogen atoms are omitted for clarity.

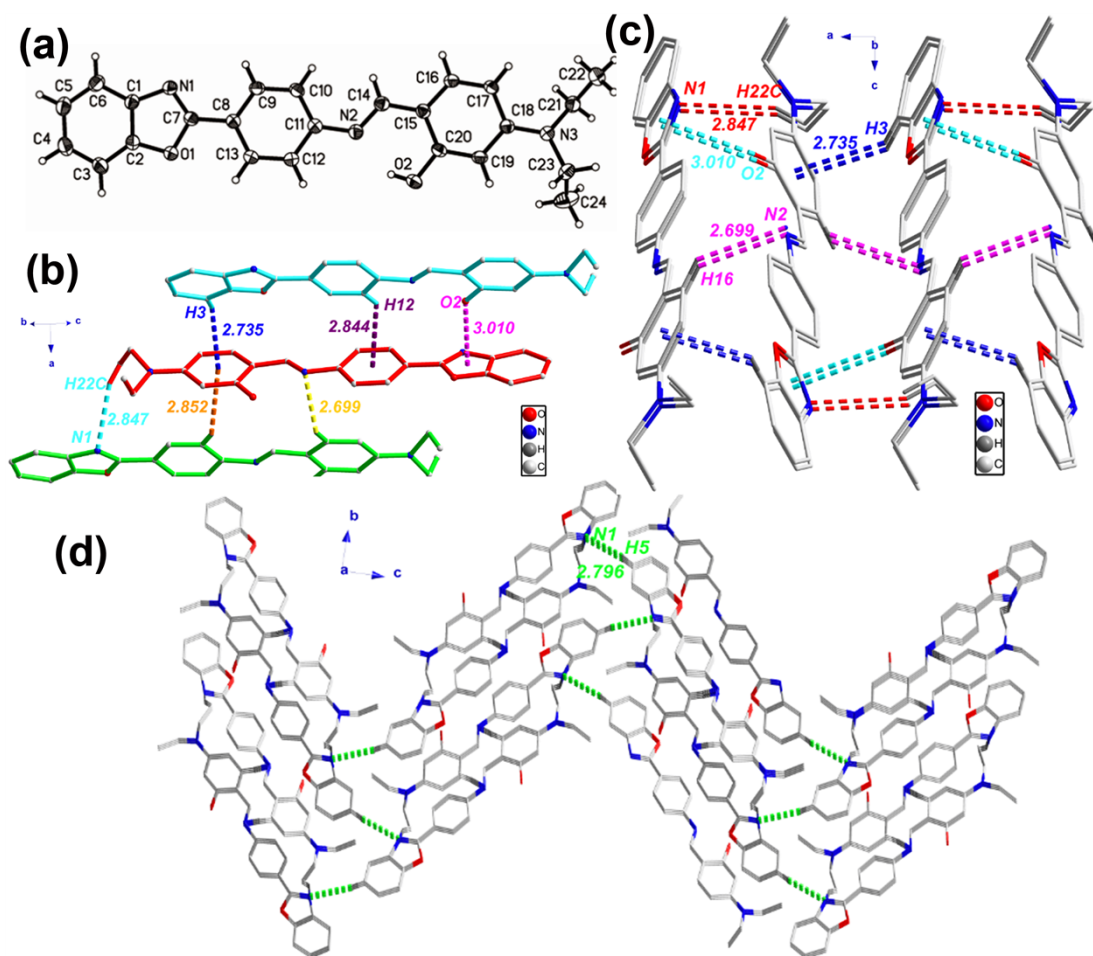


Figure S9. (a) ORTEP drawing of **2c**. (b) The one dimensional band structure of **2c** via multiple intermolecular  $\pi \cdots \text{H}$ ,  $\pi \cdots \text{O}$  and hydrogen bonds interactions. (c) Two dimensional band structure of **2c** in the crystal structure. (d) Three dimensional W-shaped stacking structure of **2c** in the crystal structure. Dotted colorful lines represent the weak interactions. Hydrogen atoms not participating in hydrogen bonds are omitted for clarity.

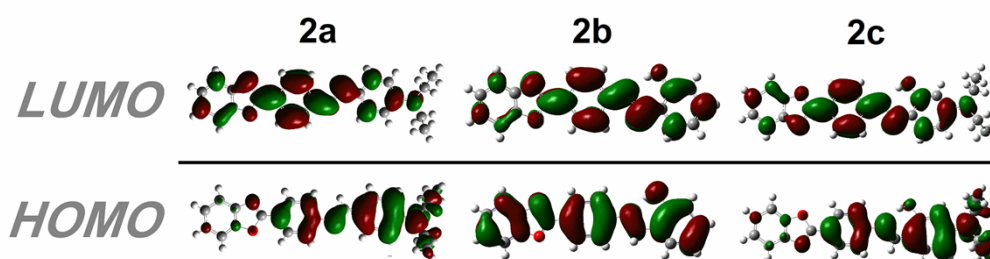


Figure S10. The B3LYP/6-31G calculated molecular orbital amplitude plots of HOMO and LUMO levels of **2a-2c**.

Table S2. Excitation energies (E), oscillator strengths (f), corresponding wavelengths ( $\lambda_{abs}$ ) and major contributors for **2a-2c**.

Compounds	E(eV)	f	$\lambda_{abs}$ (nm)	composition (C)	Character
<b>2a</b>	3.1224	1.4782	397.09	98(H)→99(L)(0.65407)	ICT
<b>2b</b>	3.4578	1.0810	358.56	82(H)→83(L)(0.63810)	$\pi \rightarrow \pi^*$
<b>2c</b>	3.1155	1.7041	397.95	102(H)→103(L)(0.64341)	ICT

Table S3. Crystallographic Data for **2a-2c**.

Compound	<b>2a</b>	<b>2b</b>	<b>2c</b>
empirical formula	C <sub>24</sub> H <sub>23</sub> N <sub>3</sub> O	C <sub>20</sub> H <sub>14</sub> N <sub>2</sub> O <sub>2</sub>	C <sub>24</sub> H <sub>23</sub> N <sub>3</sub> O <sub>2</sub>
formula weight	369.45	314.33	385.45
crystal system	Orthorhombic	Monoclinic	Orthorhombic
space group	<i>p 21 21 21</i>	<i>P2(1)/c</i>	<i>P2(1)2(1)2(1)</i>
<i>a</i> Å	7.5448(8)	26.467(5)	7.516(5)
<i>b</i> Å	9.2205(10)	4.692(5)	9.490(5)
<i>c</i> Å	28.088(3)	12.387(5)	27.807(5)
$\alpha^\circ$	90	90.000(5)	90.000(5)
$\beta^\circ$	90	101.332(5)	90.000(5)
$\gamma^\circ$	90	90.000(5)	90.000(5)
<i>V</i> Å <sup>3</sup>	1954.0(4)	1508.3(17)	1983.4(17)
<i>Z</i>	4	4	4
<i>T</i> K	296(2)	296(2)	296(2)
<i>D</i> <sub>calcd</sub> g·cm <sup>-3</sup>	1.256	1.384	1.291
$\mu$ mm <sup>-1</sup>	0.078	0.091	0.084
$\theta$ range °	1.45- 26.99	0.78- 24.99	2.27-25.00
total no. data	15269	10120	14210
no.unique data	4036	2656	3485
no. params refined	254	218	265
<i>R</i> <sub>1</sub>	0.0343	0.0509	0.0339
<i>wR</i> <sub>2</sub>	0.0964	0.1700	0.1070
GOF	1.013	1.140	0.856

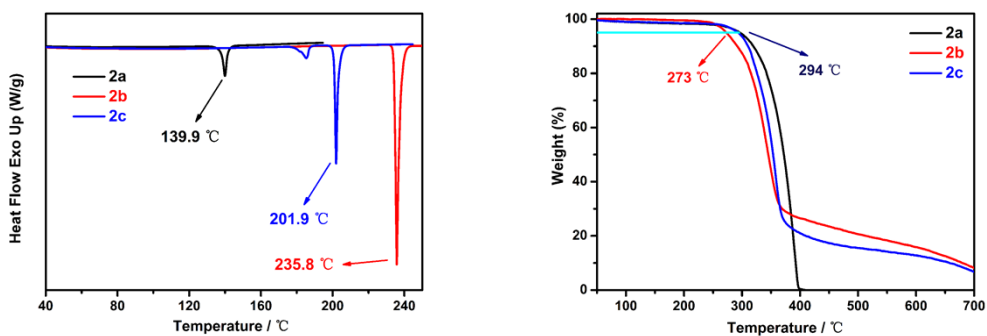


Figure S11. DSC thermograms of **2a**, **2b** and **2c**, heating rate: 20 K·min<sup>-1</sup>, atmosphere: N<sub>2</sub>. TGA thermograms of **2a**, **2b** and **2c**, recorded after pre-warming at 120 °C for 10 min under nitrogen at a heating rate of 20 K·min<sup>-1</sup>.



Figure S12. On/off fluorescence switching of **2b** nanoaggregates on the TLC plate without vapor (left) and in vapor (dichloromethane) (right) under UV light (365nm) illumination at room temperature.

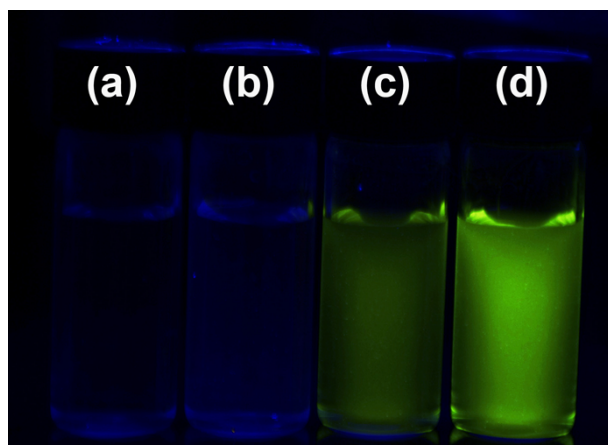


Figure S13. The photos taken under UV light of **2b** in different concentrations (a) 10 $\mu$ M, (b) 5 $\mu$ M, (c) 1 $\mu$ M, (d) 0.1 $\mu$ M with  $f_w = 80\%$  depicts the changes of PL intensity.

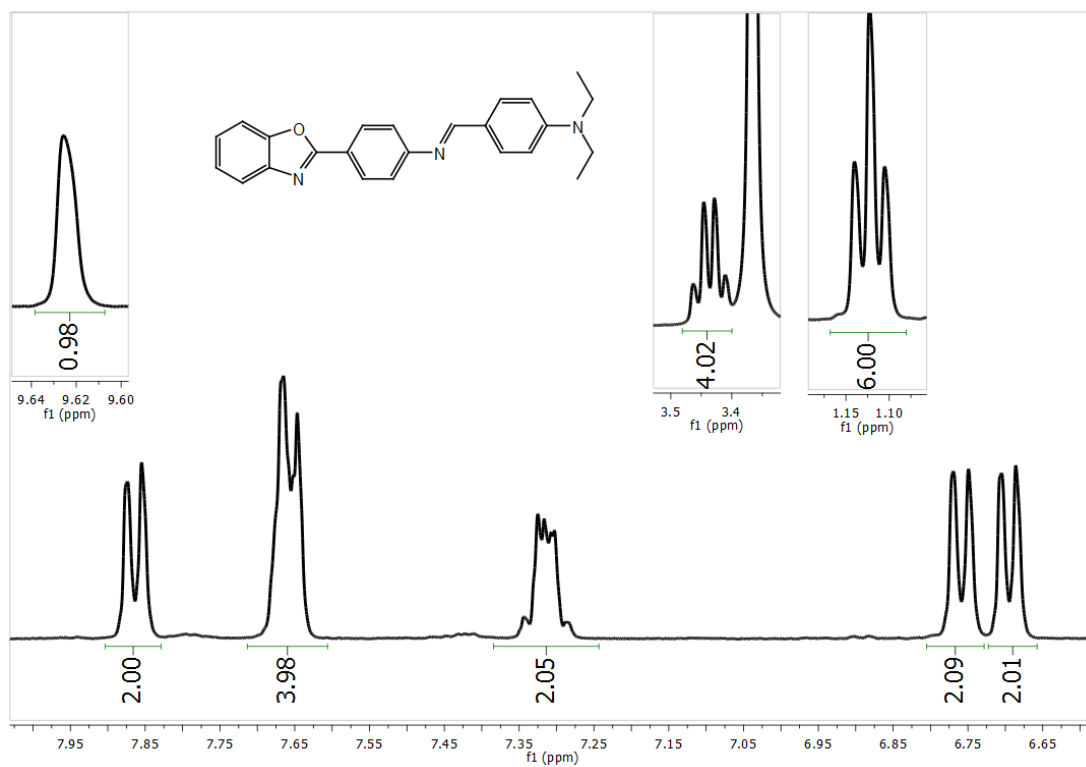


Figure S14.  $^1\text{H}$  NMR spectrum of **2a**.

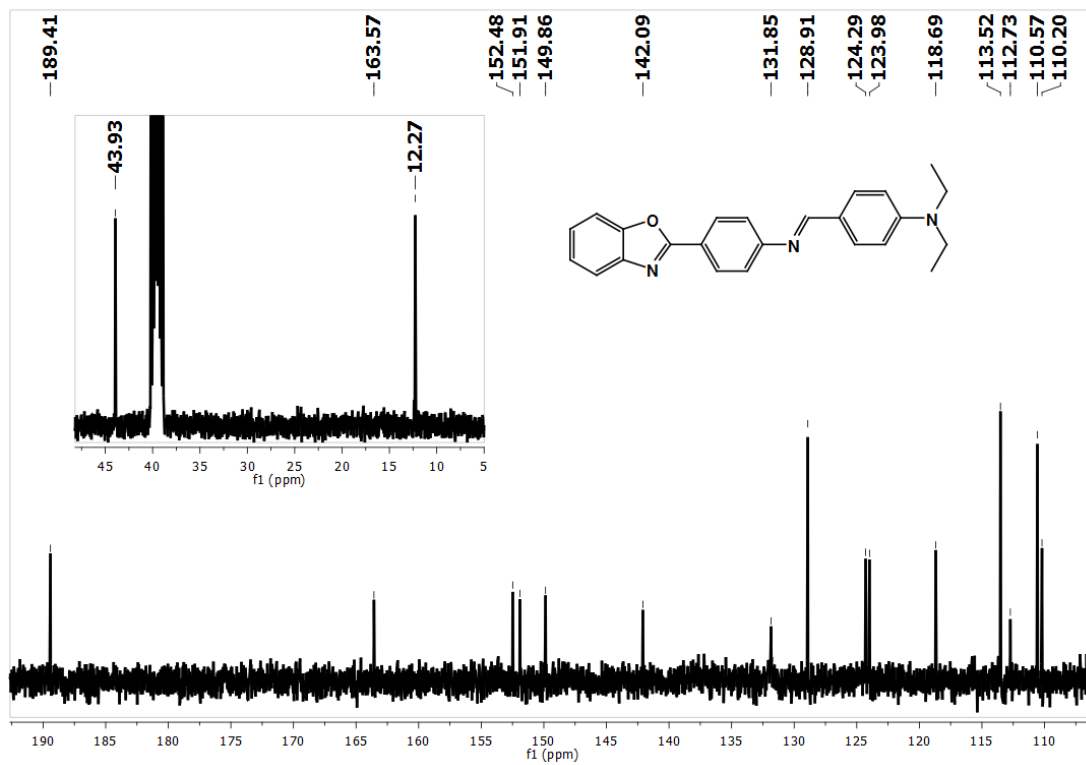


Figure S15. <sup>13</sup>C NMR spectrum of **2a**.

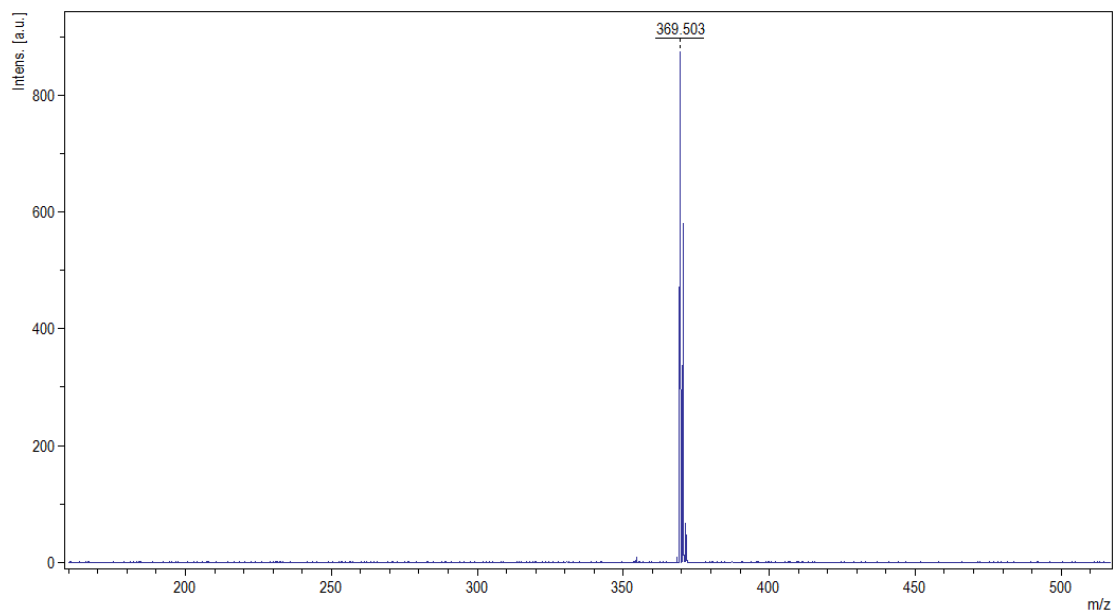


Figure S16. MS spectrum of **2a**.

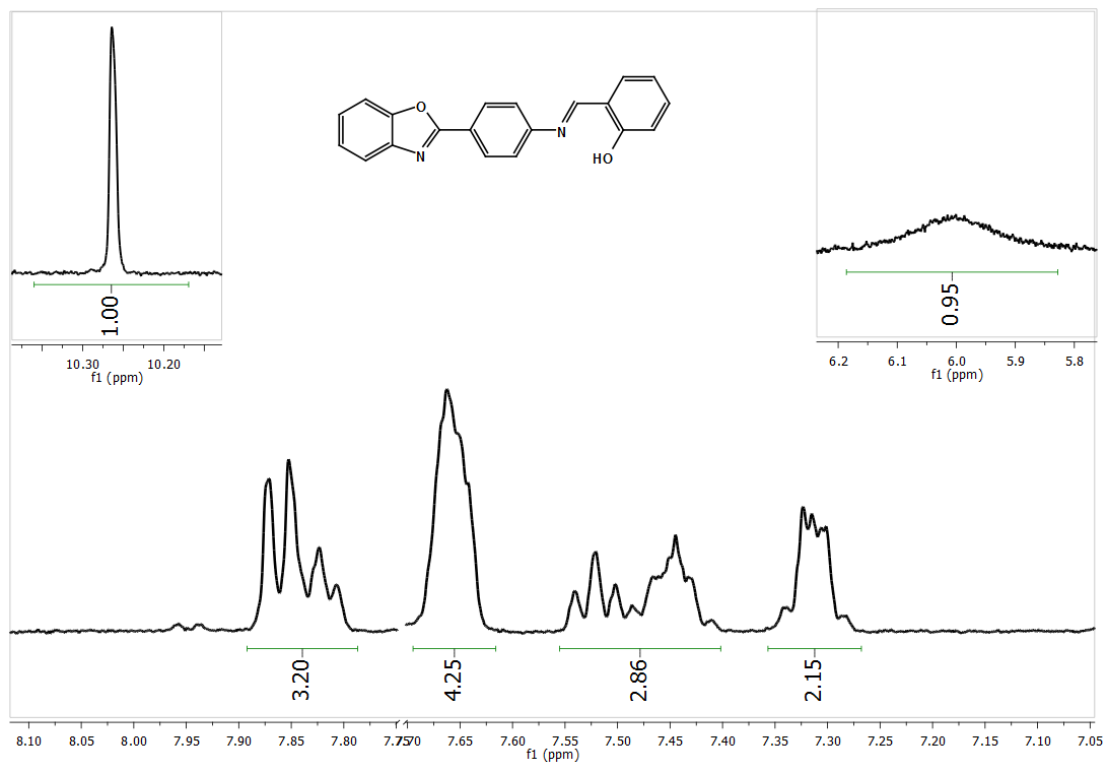


Figure S17. <sup>1</sup>H NMR spectrum of **2b**.

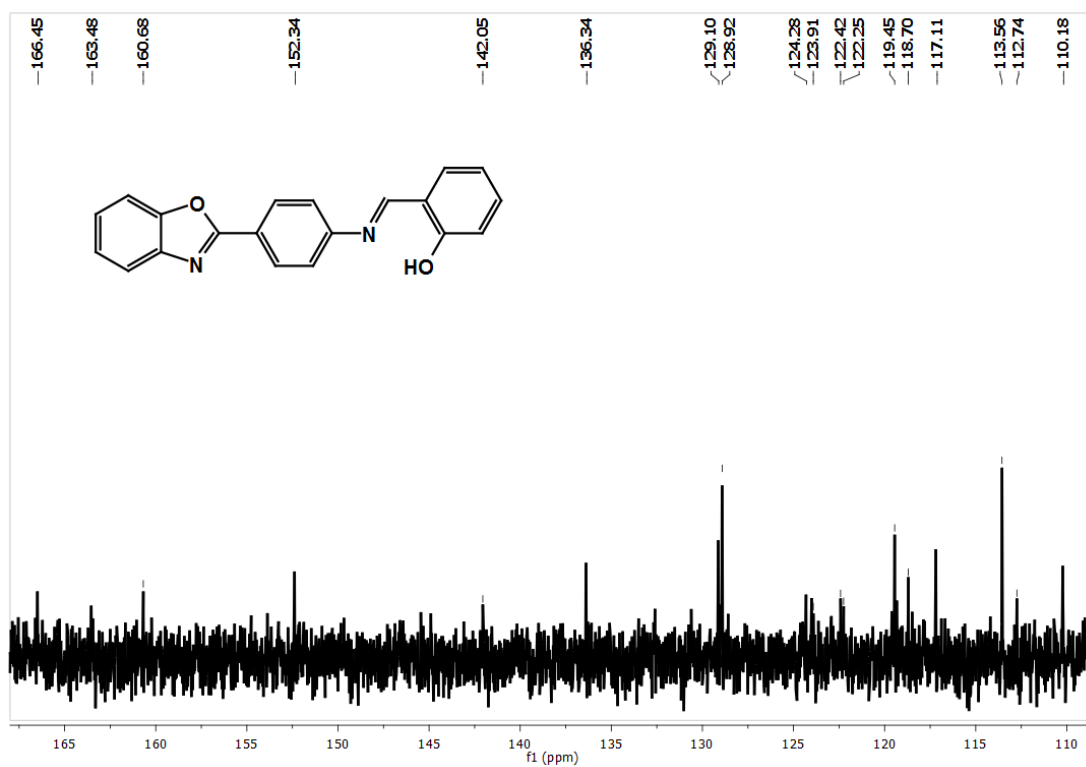


Figure S18. <sup>13</sup>C NMR spectrum of **2b**.

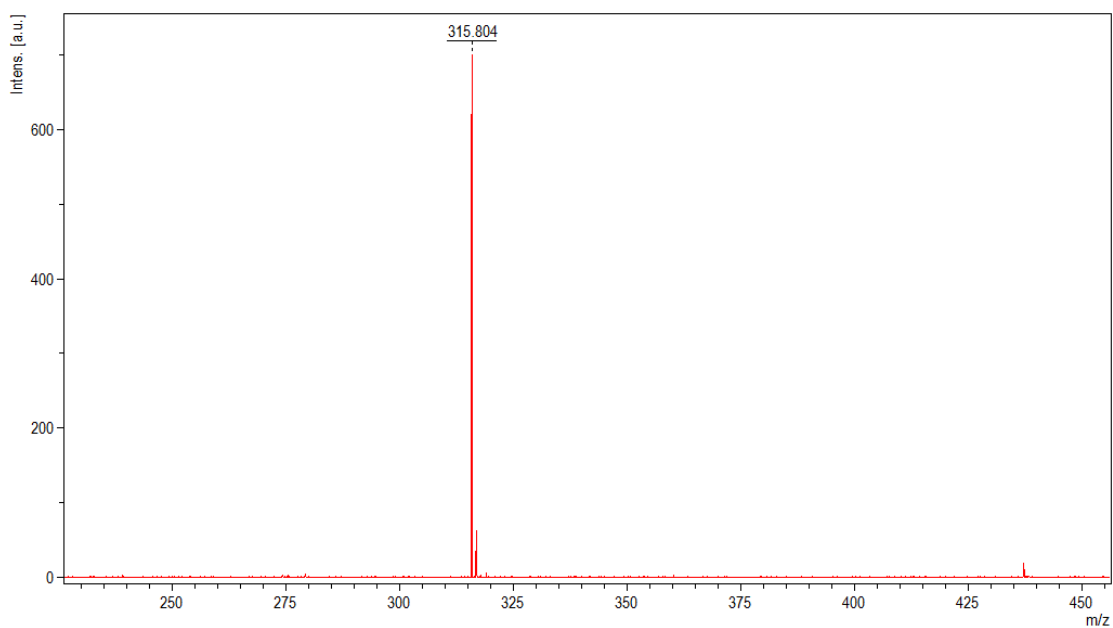


Figure S19. MS spectrum of **2b**.

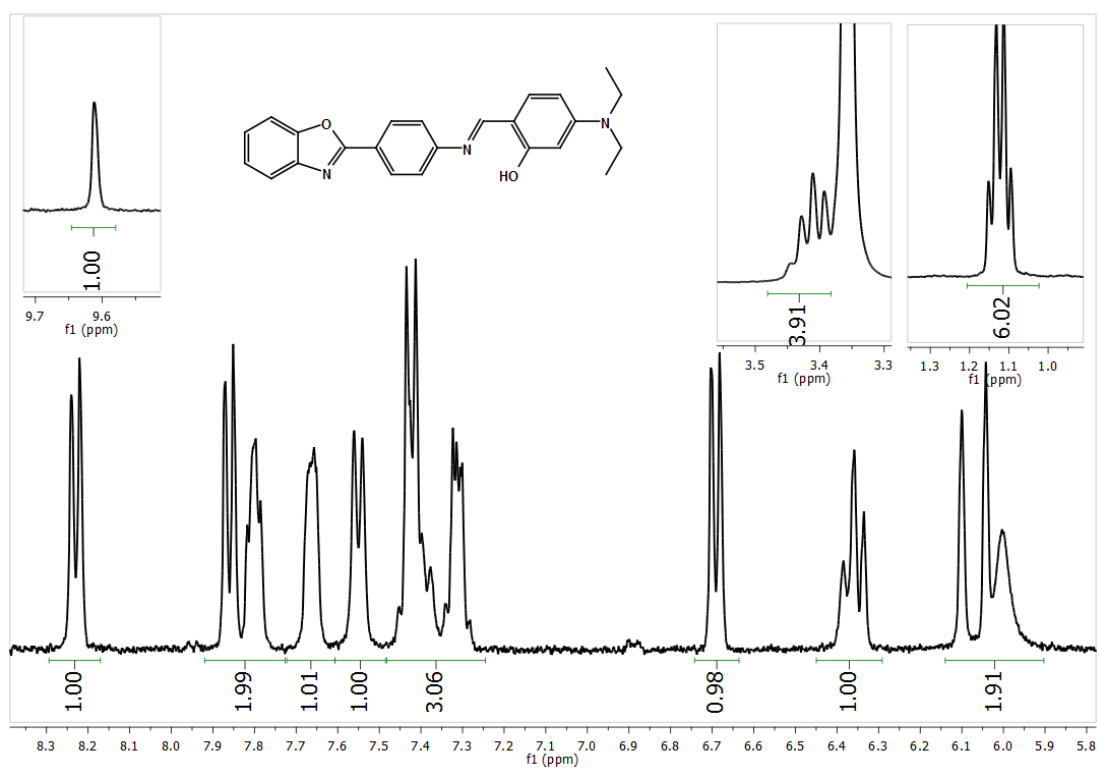


Figure S20. <sup>1</sup>H NMR spectrum of **2c**.

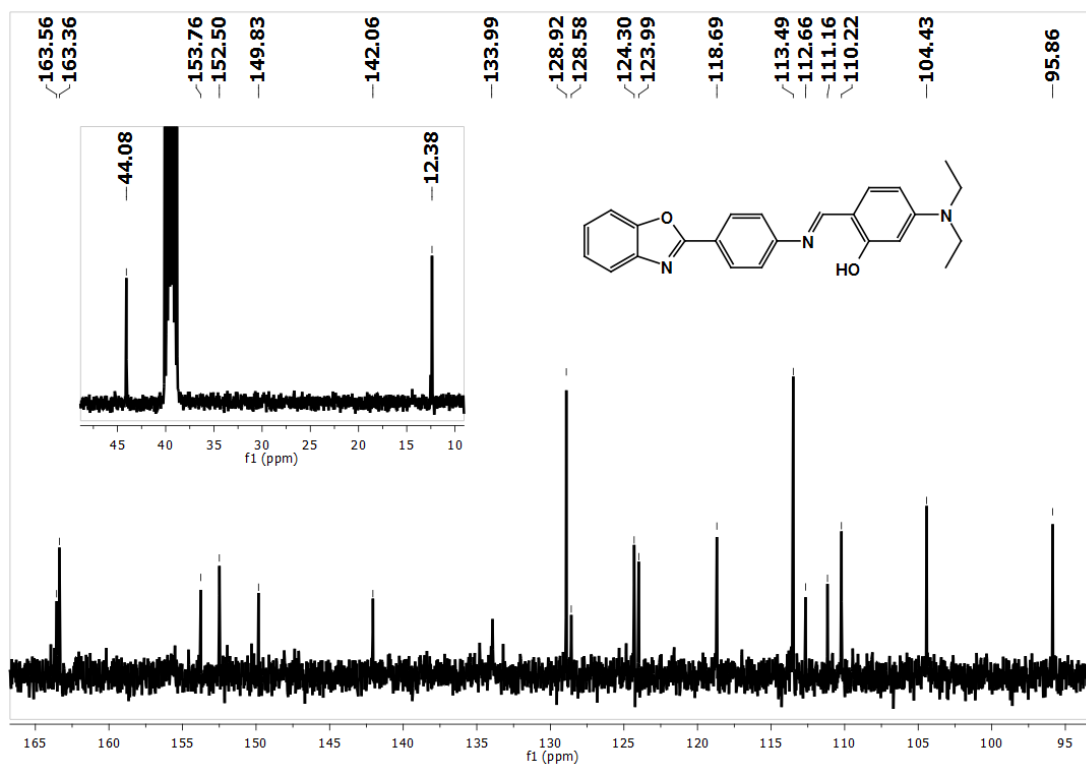


Figure S21. <sup>13</sup>C NMR spectrum of **2c**.

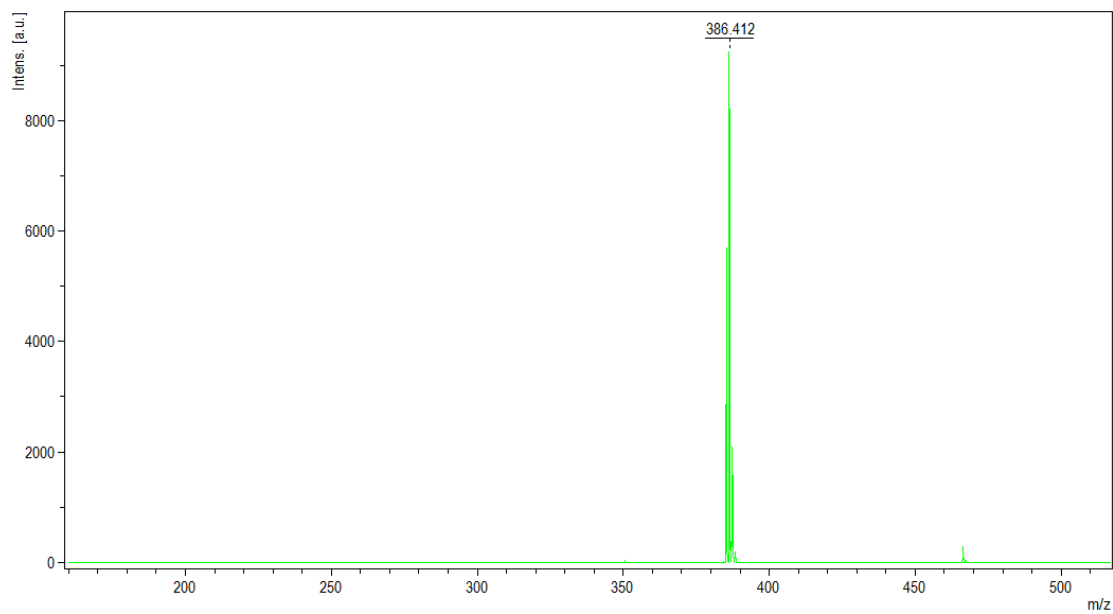


Figure S22. MS spectrum of **2c**.